AGU PUBLICATIONS

JGR

Journal of Geophysical Research: Solid Earth

RESEARCH ARTICLE

10.1002/2015JB012437

Key Points:
- We fit friction data from 1–3 order velocity steps on simulated gouge
- Stress-dependent and Slip state evolution laws fit the data well
- The Slip law does it with one fewer parameter

Supporting Information:
- Figures S1 and S2 and Text S1

Correspondence to:
P. Bhattacharya,
pathikri@princeton.edu

Citation:
Bhattacharya, P., A. M. Rubin, E. Bayart, H. M. Savage, and C. Marone (2015), Critical evaluation of state evolution laws in rate and state friction: Fitting large velocity steps in simulated fault gouge with time-, slip-, and stress-dependent constitutive laws, *J. Geophys. Res. Solid Earth*, *120*, doi:10.1002/2015JB012437.

Received 8 AUG 2015
Accepted 11 AUG 2015
Accepted article online 14 AUG 2015

Critical evaluation of state evolution laws in rate and state friction: Fitting large velocity steps in simulated fault gouge with time-, slip-, and stress-dependent constitutive laws

Pathikrit Bhattacharya[1], Allan M. Rubin[1], Elsa Bayart[2], Heather M. Savage[3], and Chris Marone[4]

[1]Department of Geosciences, Princeton University, Princeton, New Jersey, USA, [2]The Racah Institute of Physics, The Hebrew University of Jerusalem, Jerusalem, Israel, [3]Lamont-Doherty Earth Observatory, Columbia University, Palisades, New York, USA, [4]Department of Geosciences, Pennsylvania State University, State College, Pennsylvania, USA

Abstract The variations in the response of different state evolution laws to large velocity increases can dramatically alter the style of earthquake nucleation in numerical simulations. But most velocity step friction experiments do not drive the sliding surface far enough above steady state to probe this relevant portion of the parameter space. We try to address this by fitting 1–3 orders of magnitude velocity step data on simulated gouge using the most widely used state evolution laws. We consider the Dieterich (Aging) and Ruina (Slip) formulations along with a stress-dependent state evolution law recently proposed by Nagata et al. (2012). Our inversions confirm the results from smaller velocity step tests that the Aging law cannot explain the observed response and that the Slip law produces much better fits to the data. The stress-dependent Nagata law can produce fits identical to, and sometimes slightly better than, those produced by the Slip law using a sufficiently large value of an additional free parameter c that controls the stress dependence of state evolution. A Monte Carlo search of the parameter space confirms analytical results that velocity step data that are well represented by the Slip law can only impose a lower bound on acceptable values of c and that this lower bound increases with the size of the velocity step being fit. We find that our 1–3 orders of magnitude velocity steps on synthetic gouge impose this lower bound on c to be 10–100, significantly larger than the value of 2 obtained by Nagata et al. (2012) based on experiments on initially bare rock surfaces with generally smaller departures from steady state.

1. Introduction

The proper description of the evolution of the "state" variable in rate and state friction (RSF) remains an unresolved problem as none of the existent mathematical formulations agree with the full range of experimental data [*Ruina*, 1983; *Beeler et al.*, 1994; *Marone*, 1998a; *Karner and Marone*, 2001; *Bayart et al.*, 2006]. This makes the formulation of predictive numerical models of earthquake nucleation very difficult, as different state evolution laws can lead to very different nucleation styles [*Ampuero and Rubin*, 2008]. These different nucleation styles arise from the differences in the response of the sliding surface to large and rapid velocity increases, as the nucleation zone expands into regions that previously had been slipping very slowly. Thus, the propagating edge of a nucleation zone undergoes a velocity history similar to that imposed during laboratory velocity step experiments, making such experiments very relevant to studies of earthquake nucleation [*Ampuero and Rubin*, 2008; *Bhattacharya and Rubin*, 2014]. However, with a few exceptions [*Ruina*, 1983; *Tullis and Weeks*, 1986; *Bayart et al.*, 2006], laboratory velocity step increases have been typically limited to at most a single order of magnitude, in part because of the inherent difficulty in stabilizing larger velocity excursions. These velocity steps are far smaller than the multiple orders of magnitude excursions encountered in numerical simulations. Such data sets are therefore ill equipped to tell us which law to use for realistic simulations of earthquake nucleation.

In this paper, we present some of the largest velocity step laboratory data published to date, consisting of 1–3 orders of magnitude steps on simulated fault gouge. Simulated gouge is particularly suited for our experimental goals because it generally has a larger slip-weakening distance than bare rock (a larger value of the parameter D_c introduced in section 2), making it easier to stabilize large velocity steps. We carry out nonlinear

and Bayesian parameter inversions on this data set using the most common formulations of state evolution, the Dieterich (Aging) and the Ruina (Slip) laws, as well as a recently proposed state evolution law which accounts for an apparent dependence of state upon shear stress [*Nagata et al.*, 2012].

2. Background

RSF describes frictional resistance as a function of slip rate (V) and state (θ). The state variable is a measure of the total strength of the asperities bridging the sliding surface at a reference slip speed, expressed either as average contact lifetime using units of time [*Dieterich*, 1979, 1981] or in terms of contact strength using units of stress [*Nakatani*, 2001]. The relationship of the frictional resistance to the rate and state variables is given by the friction law:

$$\frac{\tau}{\sigma} = \mu(V,\theta) = \mu_* + a\log\frac{V}{V_*} + b\log\frac{\theta}{\theta_*}, \tag{1}$$

where τ is frictional resistance, σ is normal stress, μ is the "rate- and state-dependent" friction coefficient, a is the "direct effect" parameter accounting for the variations in frictional strength due to changes in slip rate, and b is the "evolution effect" parameter which determines the change in friction due to evolution of state. In general, at not very high temperatures a and b are constants of the order of 0.01 [*Blanpied et al.*, 1998; *Marone*, 1998a]. The other parameters μ_*, V_*, and $\theta_* = D_c/V_*$ are the values of friction coefficient, slip rate, and state at some reference steady state.

The mathematical framework of the problem is complete with an evolution equation for θ. Generally, in the RSF literature, evolution of the state variable has been physically interpreted as changes in one or more of (A) the real area of surface contact, (B) the strength of contact junctions at a reference strain rate, or (C) in the case of granular materials the granular packing and bulk porosity [e.g., *Dieterich and Kilgore*, 1994; *Marone*, 1998a; *Beeler*, 2007; *Li et al.*, 2011]. The two most widely used mathematical descriptions of state evolution assume that these quantities, and, hence, state, can evolve only with time and/or slip

$$\text{Dieterich (Aging) law}: \dot{\theta} = 1 - \frac{V\theta}{D_c}, \tag{2a}$$

$$\text{Ruina (Slip) law}: \dot{\theta} = -\frac{V\theta}{D_c}\ln\frac{V\theta}{D_c}, \tag{2b}$$

where D_c is some characteristic slip-weakening length scale [*Dieterich*, 1978; *Ruina*, 1983]. Equation (2a) is often referred to as the Aging law, because state increases linearly with time for stationary contacts due to the presence of the "healing term" (the 1 on the right). This property of the Aging law is usually referred to as "time-dependent healing" [*Dieterich*, 1972; *Ruina*, 1983; *Beeler et al.*, 1994]. Equation (2b) is referred to as the Slip law as state evolution occurs only for slipping contacts $\left(\lim_{V\to 0}\dot{\theta} = 0\right)$. At steady state sliding ($\dot{\theta} = 0$), both laws yield $V\theta/D_c = 1$; near steady state the two laws are asymptotically identical. Everywhere in this paper, "above" and "below" steady state implies $V\theta/D_c$ greater than and less than 1, respectively.

For sufficiently stiff experimental systems, the frictional response of both bare rock and gouge to a step change in load point velocity show that stress evolves to steady state over a slip distance that is independent of the magnitude or sign of the step [*Ruina*, 1980, 1983; *Tullis and Weeks*, 1986; *Marone*, 1998a; *Blanpied et al.*, 1998; *Bayart et al.*, 2006; *Rathbun and Marone*, 2013]. Consistent with these observations, the Slip law response to a velocity step shows exponential slip-weakening behavior over a length scale that is independent of the size or sign of the step (Figure 1) [*Rice*, 1993; *Nakatani*, 2001; *Ampuero and Rubin*, 2008; *Rathbun and Marone*, 2013]. In contrast, for large velocity step increases, the Aging law shows linear slip weakening with slope $b\sigma/D_c$. Given that the stress increase upon a step increase in velocity is an increasing function of the step size, this linear slip weakening with a constant slope implies that the length scale for the evolution of the frictional strength to approach steady state increases with the size of the step (Figure 1) [*Ruina*, 1980; *Nakatani*, 2001; *Ampuero and Rubin*, 2008]. For large velocity step decreases, on the other hand, instantaneously $V\theta/D_c \ll 1$ so $\dot{\theta} \approx 1$. This allows the Aging law θ to evolve substantially over slip distances $\delta \ll D_c$ and, ultimately, reach steady state over much smaller slip distances than for velocity step increases of the same size (Figure 1). Therefore, unlike the available laboratory data, large velocity step increases and decreases show very different characteristic length scales for state evolution under the Aging law.

In contrast to velocity step tests, slide-hold-slide tests are designed to measure the rate of frictional strengthening of the slip interface during periods of at or near-zero slip [*Dieterich*, 1972]. Such experimentally

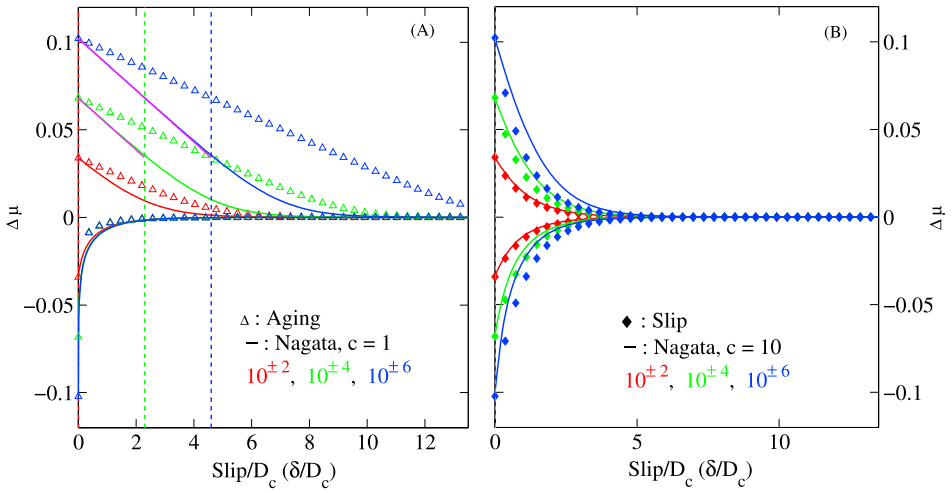

Figure 1. Analytical behavior of the Aging (open triangles in Figure 1a), Slip (solid diamonds in Figure 1b), and Nagata laws (solid curves) for velocity steps of magnitudes $10^{\pm 2-6}$. For the Nagata law, values of c are (a) 1 and (b) 10. For the Aging and Slip laws $a = b = 0.007$, $D_c = 10\,\mu$m. The scaling relations in equations (9a)–(9c) were used to obtain a, b, and D_c for the Nagata law with specified c. Note the linear slip-weakening response of the Aging law above steady state and evolution to steady state over $\delta \ll D_c$ below steady state for velocity steps $\geq 10^{\pm 2}$. The Slip law shows exponential slip weakening over the full range of velocity steps. For nonzero c one observes Slip-law-like behavior for small velocity jumps but Aging-law-like linear slip-weakening response for larger jumps. The magenta lines superposed on the Nagata law curves in Figure 1a are the slope estimates from the linear slip-weakening approximation from equation (6). The magnitude of the velocity jump required to see the Nagata law transition between Slip and Aging behavior increases as c increases. The vertical dashed lines in Figure 1a are estimates of the slip distance over which linear slip weakening occurs from equation (8). The corresponding vertical lines in Figure 1b are at almost zero slip for the range of velocity steps used. But the Nagata law response deviates from the Slip law response for velocity jumps $\gtrsim 10^{\pm 4}$ (colors correspond to the size of the jumps).

observed frictional strengthening has been widely documented as being consistent with time-dependent healing of the frictional interface [*Beeler et al.*, 1994; *Nakatani and Mochizuki*, 1996; *Berthoud et al.*, 1999]. These experimental observations of time-dependent healing have been traditionally interpreted as providing experimental support to the Aging law [*Beeler et al.*, 1994]. In particular, slide-hold-slide experiments on quartzite and granite show that the peak stresses following reslides after long holds evolve linearly with log[hold time] with a slope that is independent of machine stiffness. This feature is shared by the Aging law, where during long holds $\dot{\theta} \sim 1$ independent of the machine stiffness, but not the Slip law [*Beeler et al.*, 1994]. For the Slip law, a higher stiffness leads to smaller increases in state during the load point hold (the slip speed more rapidly approaches zero), so that the peak stress increases more slowly with log[hold time] than for a lower stiffness machine. However, this apparent experimental support for time-dependent healing as embodied by the Aging law may be negated by the fact that, again, because of the healing term, the Aging law predicts stiffness-independent evolution of the stress minima at the end of long holds, which is not observed in the data. The observed stiffness dependence in the stress minima are in much closer agreement with predictions of the Slip law. We leave a discussion of slide-hold-slide experiments to a separate paper [*Bhattacharya et al.*, 2014].

Recently, *Nagata et al.* [2012] carried out a series of "shear stress step" experiments on initially bare rock which were designed to produce very little state evolution across the step in order to estimate the direct effect term a without recourse to a particular state evolution law. They further complemented their mechanical data by measuring the variations in acoustic transmissivity across the slipping interface as a proxy for variations in the state variable. Combining their independent estimate of state with the mechanical data from their shear stress steps, they estimated a to be ~0.05, much larger than the usual estimate of $a \lesssim 0.01$. Both the Slip and Aging laws failed to fit their laboratory data with such a large value of a. To address this problem, *Nagata et al.* [2012] modified the Aging law by including a dependence upon stressing rate:

$$\text{Nagata law}: \ \dot{\theta} = 1 - \frac{V\theta}{D_c} - \frac{c}{b}\theta\frac{\dot{\tau}}{\sigma}. \tag{3}$$

Here c is another material parameter and all other symbols carry over their respective meanings (but not necessarily values) from equations (1) and (2a). The physical origin of such a stressing rate term in the state evolution equation is unclear, but its mathematical form implies instantaneous state evolution across a velocity step [*Nagata et al.*, 2012; *Bhattacharya and Rubin*, 2014]. In terms of a physical picture, it is conceivable that such rapid changes in state could be related to an instantaneous change in contact area brought about by elastic deformation of contact asperities under rapid stressing [*Nagata et al.*, 2012] (assuming no contact area change, the stress change on the asperities is larger than the applied stress change by the ratio of the nominal to true contact area, raising the possibility of finite strains). Under steady state sliding, this stressing rate term plays no role and the Nagata law predicts $V\theta/D_c = 1$, similar to the Aging (and Slip) law. The stressing rate term vanishes for $c = 0$ as well, leading to purely Aging law state evolution. *Nagata et al.* [2012] found $c = 2$ fit their data reasonably well.

The authors concluded, with support from numerical simulations, that the addition of the stressing rate term led to a quasi-symmetric response to velocity step tests [*Nagata et al.*, 2012], similar to the Slip law. When viewed alongside the fact that equation (3) retains the healing term from the Aging law, this suggests that the Nagata law might be able to explain the full range of robust observations from rock friction experiments better than either the Aging or the Slip laws. In comparison to the Aging and Slip laws, the stress-dependent formulation of state evolution is based more directly on micromechanical observations of the sliding interface [*Nagata et al.*, 2012, 2014]. This makes it important to ascertain to what extent the Nagata law explains large velocity step data and, therefore, decide whether this new, "physical" insight into friction can be utilized in earthquake nucleation simulations.

3. Response of the Nagata Law to Velocity Steps

As mentioned in section 2, when a fault surface is subjected to a step change in sliding velocity, both the Aging and Slip laws predict no instantaneous change in state. But under the Nagata law, the stressing rate term does produce an instantaneous change in state, opposite in sign to the velocity change, given any $c \neq 0$. In this section, we evaluate the implications of this shear stress dependence on state evolution by analyzing the Nagata law response to velocity steps. Under the Nagata law, the exact expression for the variation of stress with slip following a step in sliding speed is given by [*Bhattacharya and Rubin*, 2014] as

$$\Delta\tau(\delta) = b\sigma \ln\left[1 - \left\{1 - \frac{V_i\theta_i}{D_c}\left(\frac{V_f}{V_i}\right)^r\right\}\exp\left(-\frac{\delta}{D_c(1+c)}\right)\right], \tag{4}$$

where δ is slip since the velocity step; V_f and V_i are the final and initial slip rates, respectively; $\Delta\tau$ is measured with respect to the future steady state stress corresponding to the sliding rate V_f; and θ_i is the value of the state variable immediately prior to the step. The exponent r is

$$r = 1 - \frac{c}{c+1}\frac{a}{b}. \tag{5}$$

For the Aging law ($c = 0$), $r = 1$. For $c \gg 1$, $r \to 0$ (for a fixed velocity dependence of steady state friction $a-b$, we justify below that $a/b \to 1$ as $c \to \infty$).

In laboratory velocity step experiments, it is generally the case that the velocity changes are imposed on a surface previously sliding at steady state ($V_i\theta_i/D_c = 1$). With this simplification *Bhattacharya and Rubin* [2014] found the following two useful limiting forms of equation (4), depending upon the value of $(V_f/V_i)^r$: $(V_f/V_i)^r \gg 1$:

$$\Delta\tau \approx b\sigma\left(1 - \frac{c}{c+1}\frac{a}{b}\right)\ln\left(\frac{V_f}{V_i}\right) - \frac{b\sigma}{D_c(1+c)}\delta, \quad \delta < N[D_c(c+1)]\,; \tag{6}$$

$(V_f/V_i)^r \sim 1$:

$$\Delta\tau(\delta) \approx b\sigma\left(1 - \frac{c}{c+1}\frac{a}{b}\right)\ln\left(\frac{V_f}{V_i}\right)\exp\left(-\frac{\delta}{D_c(1+c)}\right). \tag{7}$$

These equations show how the response of the Nagata law to velocity steps can mimic either the Aging law or the Slip law, depending upon c and the amplitude of the velocity step. Equation (6) exhibits linear

slip-weakening behavior, similar to the Aging law, up to slip distances of N times $D_c(c+1)$ during the approach to steady state, where N is given roughly by

$$\left(\frac{V_f}{V_i}\right)^r \exp(-N) \approx \mathcal{O}(10). \tag{8}$$

The slip-weakening rate, given by the second term on the right, is $b\sigma/[D_c(1+c)]$, compared to $b\sigma/D_c$ for the Aging law. Considering the requirement for the applicability of equation (6), $(V_f/V_i)^r \gg 1$, *Bhattacharya and Rubin* [2014] showed that for any given value of c, there exists a critical value of V_f/V_i above which the Nagata law response shows linear slip-weakening behavior, similar to the Aging law, and that the size of this critical velocity jump increases with the value of c. For velocity decreases as large as the increases that satisfy equation (6), the Nagata law shows effects of time-dependent healing with substantial state evolution occurring over $\delta \ll D_c(c+1)$. This leads to steady state being attained over much smaller slip distances than velocity increases of the same size, similar to the Aging law response (Figure 1).

For velocity jumps of either sign much smaller than this critical size, $(V_f/V_i)^r \sim 1$ and equation (7) applies. This equation exhibits exponential decay of stress over a characteristic slip distance independent of the sign or size of the jump, just as for the Slip law. In fact, this limiting form of the Nagata law is identical to the response of the Slip law to velocity steps, given a set of scaling relationships between the Nagata and Slip law parameters described in equations (9a)–(9c) below. Furthermore, although mathematically for any finite c there is some value of V_f/V_i above which the Nagata law response shows linear slip-weakening behavior, for $c \gg 1$ such velocity jumps are not realizable in nature (e.g., with $c = 10$ and $a = b$, $(V_f/V_i)^r \sim 10$ requires $\log_{10}(V_f/V_i) \sim 25$). Thus, for $c = 0$ the Nagata law is identical to the Aging law, while for $c \gg 1$ the response of the Nagata law to physically plausible velocity steps is asymptotically identical to that of the Slip law.

For velocity excursions imposed from steady state, there is a simple physical interpretation of $(V_f/V_i)^r$: It equals $V_f\theta_f/D_c$, the measure of how far from steady state the surface is brought immediately following the step (we define θ_f as the value of state immediately following the velocity step). One can think of the stressing rate term in equation (3) as adjusting how far from steady state the slip surface is pushed by a given velocity jump, by controlling the amount of state evolution across the jump. Viewed in this way, the linear slip-weakening response occurs when c is small enough that the imposed velocity step can push the slip surface far above steady state, while the exponential slip-weakening response occurs when c is large enough to prevent this. These transitions are shown in Figure 1. Because the Nagata law was developed by adding a stressing rate term to the Aging law, it might be helpful to note that the exponential slip-weakening response when the fault is close to steady state can be viewed as the near steady state response of the Aging law, since the Slip and Aging laws are asymptotically identical near steady state [*Bhattacharya and Rubin*, 2014, Appendix C].

To complete the discussion of the response of the Nagata law to velocity step tests, we tabulate three scaling relationships that describe the exact correspondence between the Slip and Nagata law parameters when equation (7) holds:

$$D_c(1+c)|_{\text{Nagata}} \equiv D_c|_{\text{Slip}}, \tag{9a}$$

$$\frac{a}{1+c}|_{\text{Nagata}} \equiv a|_{\text{Slip}}, \tag{9b}$$

$$(a-b)|_{\text{Nagata}} \equiv (a-b)|_{\text{Slip}}. \tag{9c}$$

Equation (9a) follows from equation (7) because the characteristic slip-weakening distance, which is a property of the frictional interface, is $D_c(1+c)$ for the Nagata law instead of D_c for the Slip law. Equation (9b) follows from the requirement of having the same peak stress value for the Nagata and Slip laws following a given velocity step up/down and indicates why the larger a values observed in experiments carried out by *Nagata et al.* [2012] could be accommodated by introducing the stressing rate term. Equation (9c) follows from the requirement to have the same amount of steady state velocity weakening/strengthening independent of the state evolution law. These scaling relations along with equation (7) tell us that if a velocity step data set is closely fit by the Slip law, then we can always find a value of c large enough for the Nagata law to match the data equally well. But, importantly, all values of c larger than this critical value will also fit this data set equally well but with a, b, and D_c now scaled according to equations (9a)–(9c). Therefore, velocity step data well explained by the Slip law cannot fix the value of c to any better than a lower bound.

Finally, we have the following expression for a/b given a constant value of $b - a = \Delta$:

$$\frac{a}{b}\Big|_{\text{Nagata}} = \frac{a|_{\text{Slip}}(1+c)}{a|_{\text{Slip}}(1+c)+\Delta}. \tag{10}$$

Therefore, for a given value of Δ, $a/b \to 1$ for $c \gg 1$. The scaling relationships in equations (9) and (10) are observed to hold quite well when fitting the same set of velocity step up/down data with both the Nagata and the Slip laws (section 4.2 and Appendix B).

We note that this discussion reinforces the importance of obtaining laboratory velocity step data with velocity excursions as far from steady state as possible. Existing experiments are consistent with exponential slip weakening over a length scale independent of the magnitude of the velocity step, consistent with the Slip law. But the Nagata law, motivated by an indirect measure of the state variable, predicts that for any given c the response of the fault surface will transition from Slip-law-like to Aging-law-like as the velocity jump increases. If this transition occurs at less than elastodynamic speeds, as it would for the value $c = 2$ inferred by *Nagata et al.* [2012], it will influence the style of earthquake nucleation [*Bhattacharya and Rubin*, 2014]. Nonetheless, such a Slip law-Aging law transition has not been observed in the laboratory. The experiments of *Nagata et al.* [2012] are limited to modest excursions from steady state; those we describe below include excursions up to nearly 3 orders of magnitude.

4. Fitting Laboratory Data

On the basis of the discussion in section 3, it is reasonable to expect that a velocity step up/down data set which is well fit by the Slip law can be equally well fit by the Nagata law with sufficiently large values of c. In parameter inversions with such a data set, we can only expect to find the lower bound on acceptable values of c. We further expect that this lower bound on c will increase with the size of the velocity jump, i.e., how far the sliding surface is pushed from steady state. In this section, we make use of these analytical results while performing parameter inversions on laboratory data. For all our inversions our forward model is composed of two coupled differential equations—force balance between elasticity and friction and the relevant state evolution law. Differentiating the friction law (equation (1)) with respect to time and equating this with the time derivative of the spring force, the force balance for a single degree of freedom system is

$$a\frac{\dot{V}}{V} + b\frac{\dot{\theta}}{\theta} = k(V_{lp} - V), \tag{11}$$

where V_{lp} is the load point velocity and k is stiffness normalized by the normal stress (so k has units of length^{-1}). The time-varying load point velocity is imposed by specifying the desired load point displacements as a function of time. The actual load point velocity achieved is determined from measured displacements of the load point, and the stiffness is that of an equivalent spring connecting the sliding interface to the point at which the load point displacement is measured. This stiffness is estimated from measurements made at the start of the largest velocity increases (Appendix A). We solve this forward model for a particular choice of the model parameters in order to obtain numerical values of the shear stress at all times at which the experimental shear stress was recorded. We use a weighted sum of squares (l_2 norm) of the difference between the numerical and experimental time series to quantify the misfit. The weighted root mean square error (RMSE) is also used to construct the likelihood function for Bayesian inference on the data (see the supporting information).

4.1. Experimental Setup

We used velocity step data from the experiments of *Bayart et al.* [2006] carried out in the Penn State Rock and Sediment Mechanics Lab. The experimental setup is a biaxial double-direct-shear configuration designed to measure the frictional and mechanical properties of granular materials or bare rock [*Dieterich*, 1972; *Savage and Marone*, 2007]. For all the experiments discussed here, the sample consisted of simulated granular quartz gouge. In this case, the double-direct-shear configuration consists of two layers of sample material, each 3 mm thick, sandwiched between three steel forcing blocks. The quartz particles were initially subangular and have initial grain size of 50–150 μm. Grooves cut perpendicular (0.8 mm deep and 1mm wide) to the sliding direction force shearing to occur within the layer rather than at the boundaries. Fast-acting servo-hydraulic controllers are used to maintain specified normal stress on the sliding surfaces and displacement rate on the ram. Forces are measured with load cells mounted to the end of each ram. Displacements are recorded with direct current displacement transducers mounted both at the load point and on the sample, straddling the

slip surface. The nominal frictional contact area for our experiments was 10 cm × 10 cm. All experiments were carried out at 25 MPa normal stress under ambient room humidity (43% to 57%) and temperature (23.7°C to 26.7°C). The sliding velocities accessed in these experiments ranged from 0.5 μms^{-1} to 500 μms^{-1}.

All experiments showed an initial transient regime where the "steady state" friction gradually increased up to slip distances of about 10 mm, followed by steadier behavior where the friction coefficient under steady sliding was more nearly constant. All the results that we discuss here are from experiments carried out in the latter regime, which from previous experiments in the Penn State lab corresponds to the case where well-developed shear bands have been formed within the gouge. The slip is thought to occur along a well-developed sliding interface within the shear band [e.g., *Rathbun and Marone*, 2013]. In this larger slip range the surface was very nearly velocity neutral ($a \sim b$).

4.2. Parameter Inversion

As emphasized earlier, we need our velocity step experiments to push the slip surface as far above steady state as possible in order to fully explore the part of the parameter space most relevant to earthquake nucleation. However, owing to the finite stiffness of the experimental apparatus, a 3 orders of magnitude velocity step imposed at the load point does not translate to a 3-order velocity step on the sliding surface and, therefore, does not drive the surface as far from steady state as desired. Additionally, to qualitatively assess the successes or failures of the various laws, it turns out to be useful to compare the data and the fits to the analytical expectations that arise from "true" velocity steps (e.g., do the data support linear slip weakening with a fixed slope, or exponential slip weakening over a fixed length scale, in both cases independent of the size of the jump?).

4.2.1. Velocity Steps of Up to 2 Orders of Magnitude

One way to bypass the limitations of finite stiffness machines and produce more accurate velocity steps is to servo-control the load point off a displacement transducer straddling the slip surface [*Ruina*, 1980, 1983; *Linker and Dieterich*, 1992; *Bayart et al.*, 2006]. In practice this means that the ram displacement is continually adjusted to negate any difference between the displacement measured close to the fault and the desired displacement history on the slip surface. Using this approach, we were able to stabilize 1–2 orders of magnitude velocity step ups/downs (data set p1060) and produced a close to ideal data set to compare with analytical results [*Bayart et al.*, 2006]. Bayart et al. showed that the Slip law does a very good job of fitting the shear stress evolution for this data set (Figure 2). On the other hand, besides producing a fit worse than the Slip law to the velocity step increases, the best fitting Aging law does a particularly poor job with the large velocity step downs. This is because the Aging law, with its time-dependent healing, predicts too much state evolution over $\delta \ll D_c$ following the velocity decreases. Therefore, given large perturbations to steady state sliding, the Slip law explains laboratory velocity step data much better than the Aging law. Furthermore, since these experiments drive the sliding interface further from steady state than the experiments of *Nagata et al.* [2012], our analytical results suggest that fitting the data as closely as the Slip law might require values of c larger than the value ($c = 2$) that they found.

For preliminary inversions, we employed a downhill simplex scheme [*Press et al.*, 1996] initiated with parameter values dictated by various trends in the data. We used time-varying weights along the misfit time series in order to calculate the RMSE values. The strategies adopted in designing such schemes are described in the supporting information. For most of our inversions we fix $a - b \approx -0.0002$ based on the behavior at steady state, and stiffness (between the sliding surface and the loading ram) $k = 0.0011\ \mu m^{-1}$ based on the short-term stress response to the largest load point velocity increase (Figure A1 in Appendix A). The fits for the Aging, Slip, and Nagata laws are shown in Figure 2a. Even though the misfit was calculated between the observed and modeled stress time series, we plot the fits and the stress data against fault slip, rather than time, to facilitate comparisons with the analytical results for velocity steps. The data are plotted against fault slip calculated as $\delta = \delta_{lp} - \Delta\mu/k$, where δ_{lp} and $\Delta\mu$ are the observed load point displacement and friction coefficient (shear stress divided by normal stress), respectively. The modeled friction coefficient is plotted against the fault slip as determined by the forward model. Figure 2b compares the slip velocity obtained by differentiating the fault slip calculated from the data ($V = \mathrm{d}\delta/\mathrm{d}t$) with the slip velocities predicted by the respective state evolution law fits shown in Figure 2a. The best fitting Slip and Nagata laws evidently also explain the slip velocity data most closely. For the Nagata law the downhill simplex algorithm gets trapped in many local minima in the parameter space depending on the starting values of c. For $c = 2$, the Nagata law does a much worse job than the Slip law. Fits similar to those produced by the Slip law were found only for $c \gtrsim 10$ by experimenting with various initial parameter values. The existence of many local minima for c above the approximate

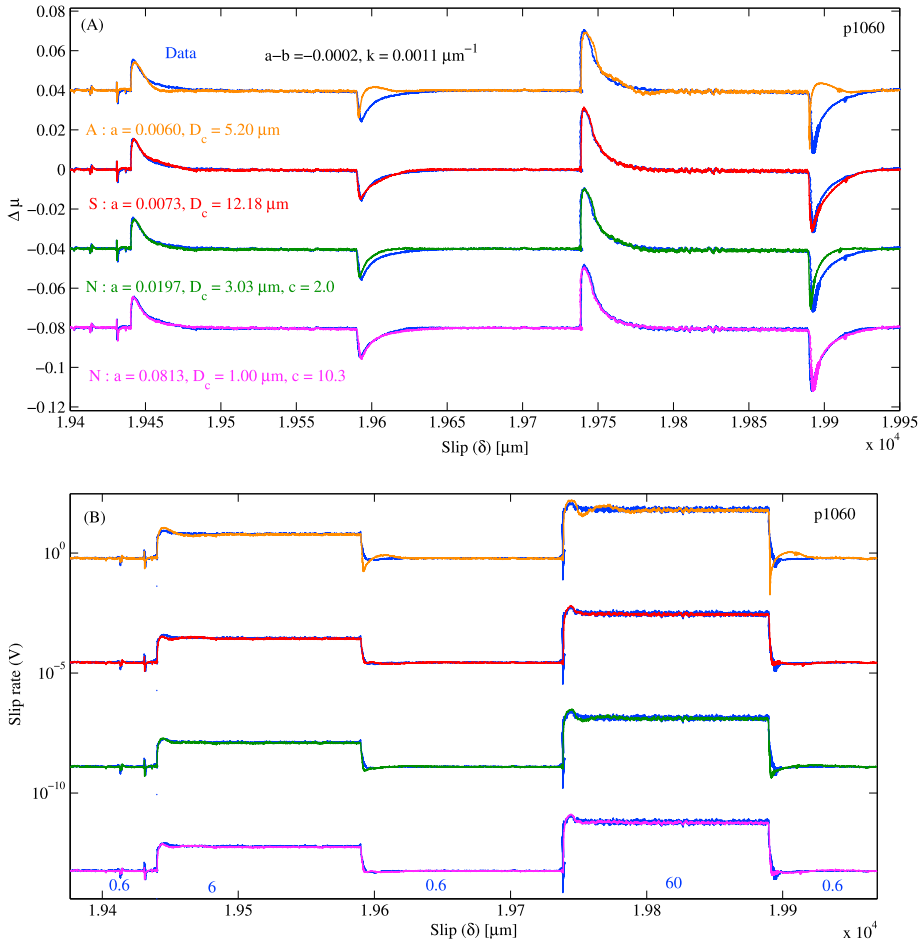

Figure 2. Results from a velocity step up/down experiment (data set p1060) carried out by servo-controlling off a displacement transducer mounted directly on the sample, hugging the sliding surface. (a) The fit to $\Delta\mu$. (b) The corresponding slip rates (V) predicted by the forward model for the best fitting $\Delta\mu$ time series with the stiffness estimated as described in text. Blue: data; ochre: Aging law; red: Slip law; green: Nagata law with $c = 2$; purple: Nagata law with $c \approx 10$. The numbers in blue in Figure 2b denote measured load point velocities in μms^{-1}. Plots are scaled and shifted to improve visibility. The Slip law does a good job of fitting the data due to its characteristic exponential slip weakening over a fixed length scale for step ups/downs of all magnitudes. The Nagata law does a slightly better job with $c \approx 10$.

lower bound of 10 is expected from the scaling relationships in equations (9a)–(9c). We also observed local minima for $c \lesssim 10$; all of these produced fits worse than the Slip law but better than the Aging law ($c = 0$).

To investigate the details of the full posterior distributions of the Nagata RSF parameters, we designed a small world Markov chain Monte Carlo global search with adaptive proposal distribution [*Rosenthal*, 2011; *Bai*, 2009a, 2009b; *Guan et al.*, 2006]. The details of this inversion scheme are given in the supporting information. The results from a typical, long Markov chain (50,000 iterations with about an initial 25% being thrown out as burn-in) derived from data set p1060 are shown in Figure 3. The most striking feature of the posterior distributions of a, D_c, and c (Figures 3a–3c) is their remarkable covariance. The interrelationships of the shapes of the three posteriors are consistent with the trends predicted in the scaling relations in equations (9a)–(9c). The posterior distribution of c shows the presence of a strongly peaked region corresponding to $c \sim 10$–100 and a quasi-uniform tail which continues to orders of magnitude larger values of c. This clearly shows the existence of many possible Nagata law fits over orders of magnitude variations in c, all of which are statistically acceptable given the specified level of data error. Our chains were truncated at some predecided upper bound of c by imposing constraints through the prior distribution. For the chain in Figure 3 this upper bound was at $c \sim 10^5$, leading to the slow falloff of the quasi-uniform tail beyond $c \gtrsim 10^4$ in Figure 3c. Upon closer inspection (Figures 3d and 3e) the fits to the data represented by the peaked region of the posterior appear

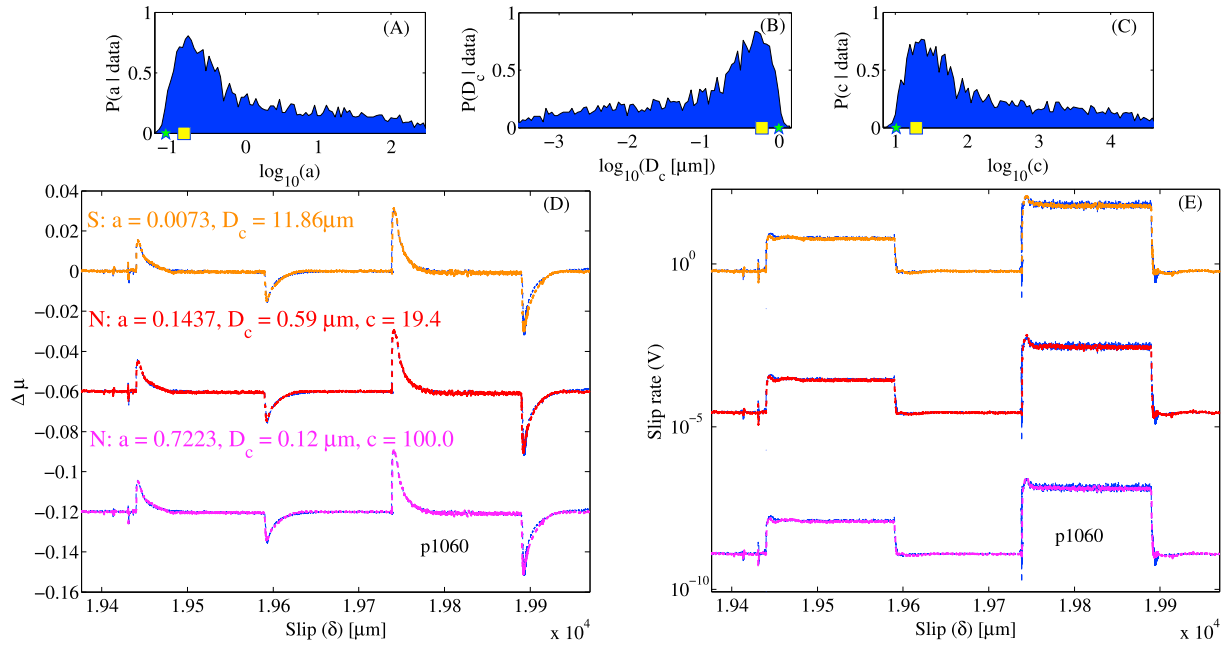

Figure 3. The marginal posteriors for the Nagata law Markov chain for the data set in Figure 2 for (a) a, (b) D_c, and (c) c. The first 2500 accepted samples were discarded to account for a burn-in period. The Markov sampling was truncated at $c = 10^5$. The posteriors are dominated by a strongly peaked region (representing fits which look slightly better than the Slip law) and a quasi-uniform tail (representing exactly Slip-law-like fits) showing that there exist infinitely many solutions at this level of data error (see Appendix B for details on estimation of data error). The green star denotes the initial point and the yellow square the least RMSE value. (d) The fit to $\Delta\mu$ values and (e) The corresponding slip rates (V) predicted by the forward models which fit the stress data. Blue: data; ochre: the best fitting Slip law; red: Nagata law with $c \approx 19.4$ which leads to the least RMSE in the Markov chain; pink: Nagata law with $c = 100$ fits the data almost exactly like the Slip law. Exact values of a and D_c for this value of c were searched by redoing a downhill simplex with the values of c and $a - b$ fixed.

not to be visually identical to the best Slip law fit. In particular, Figure 3d shows that the fit to the 2-order step down with $c \sim 20$ (which produces the global minimum of the RMSE for the chain and is typical of the fits represented by the peaked region) looks slightly better than those produced by the Slip law. The Nagata law fits that are indeed visually identical to the Slip law are found only for $c \gtrsim 100$ and are represented by the quasi-uniform tail. Therefore, for experiment p1060, there are two critical values of c that define the family of optimal Nagata law fits: (1) $c \sim 10$ represents the smallest value of c with which one can produce a Nagata law fit to p1060 that is at least as good as the best fitting Slip law; (2) $c \sim 100$ represents the lower bound on c to produce fits identical to the best fitting Slip law. We treat the statistical distinctions between these families in greater detail in Appendix B.

The absence of accepted fits to the stress data for $c \lesssim 10$ shows that in order to fit this data set at least as closely as the Slip law, the lower bound on c is ~ 10. This value is considerably larger than the $c = 2$ adopted by *Nagata et al.* [2012], who fit generally smaller departures from steady state. This supports our analytical expectation that given ever increasing laboratory velocity steps all well modeled by the Slip law, one needs to systematically increase c to produce Nagata law fits similar to those produced by the Slip law. However, the fact that the *Nagata et al.* [2012] experiments were performed on bare rock also raises the possibility that this variation in c reflects a difference between rock and gouge, an issue that we cannot address with gouge data alone. But if successively larger velocity steps on the same gouge material are all well modeled by the Slip law, this raises the question of whether introducing the extra parameter c in the Nagata law is justified for gouge. In the next section, we attempt to address this question by analyzing velocity step data containing > 2 orders of magnitude steps on the same gouge material as used in p1060.

4.2.2. Velocity Steps Larger Than 2 Orders of Magnitude

The strategy of servo-controlling the loading ram off the transducer straddling the fault was unable to stabilize velocity step increases larger than 2 orders of magnitude. To attempt larger increases, we designed a specific velocity history for the load point such that, given an estimate of the stiffness of the apparatus and the parameters of a particular state evolution law, it would produce a nearly true velocity step on the sliding surface by adjusting the load point appropriately via servo control. In our case we assumed a set of Slip

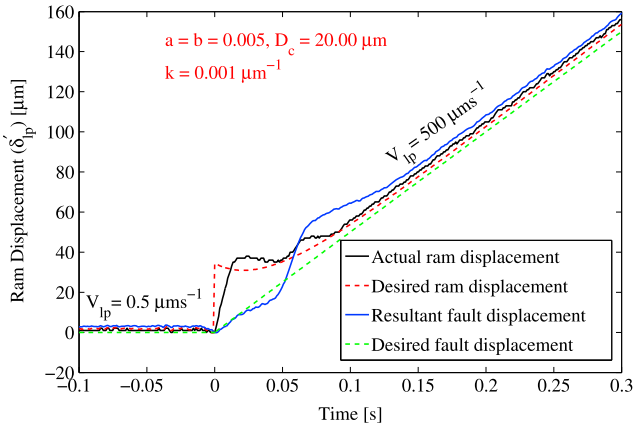

Figure 4. Slip history of the loading ram when servo-controlled off the ram transducer, with a displacement history corresponding to a desired 3 orders of magnitude velocity step increase on the sliding surface (from p1180). Red dashed line: intended ram displacement derived from the analytical solution for velocity steps under the Slip law; black solid line: actual ram displacement; blue solid line: resultant fault displacement time history; green dashed line: desired fault displacement. The assumed parameters are listed in red.

law parameters which fit previous experiments well. In practice, we used force balance and determined the change in shear stress by using the response of the Slip law to a step velocity increase [*Ampuero and Rubin*, 2008, equation (7)] to write the required load point displacement history as

$$\delta'_{lp} = \frac{a}{k}\ln\left(\frac{V_f}{V_i}\right)\left[1+\frac{b}{a}\left\{\exp\left(-\frac{V_f t}{D_c}\right)-1\right\}\right] + V_f t, \quad \delta'_{lp}, t \geq 0\,, \tag{12}$$

where δ'_{lp} and t are the ram displacement and time elapsed since the step, respectively. An example of such a ram history is shown in Figure 4, designed to impose a 3 orders of magnitude velocity increase on the sliding surface. The design includes an instantaneous change in load point displacement, to produce an instantaneous change in stress, followed by a small reversal of the load point velocity (according to equation (12)) necessary to avoid velocity overshoot due to strong frictional weakening. The actual displacement history of the ram did not strictly follow the designed history due to inherent limitations of servo control. This meant that a true velocity step could not be imposed on the fault (blue solid line in Figure 4). But even with perfect servo control, modest variations of the Slip law parameters from experiment to experiment means that the sliding histories would still not have approximated true velocity steps to any great degree of accuracy. In spite of these shortcomings, the main advantage of such designed velocity steps is that we can reasonably expect these to push the sliding surface further from steady state than "traditional" load point velocity steps of the same order of magnitude. The velocity step decreases, however, were imposed as traditional load point steps for these experimental runs.

Using such "designed" load point displacement histories, we were able to generate two other sequences of large velocity steps on simulated gouge, each of which contained attempted 3 orders of magnitude velocity step increases (Figures 5a, 5d, 6a, and 6b). Given that we did not impose a true velocity step at the sliding surface, we estimated the actual departure from steady state using a forward model that fits the data reasonably well. Assuming that the best fitting Slip law was a good approximation to the stress data, the maximum value of $V\theta/D_c$ predicted by this forward model was used as a proxy for the maximum departure from steady state following a velocity increase. Defined in this way, the largest velocity step for the data set p1169 in Figures 5c and 5d pushed the slip surface nearly 3 orders of magnitude from steady state (peak modeled Slip law $V\theta/D_c \sim 750$). For comparison, the peak $V\theta/D_c$ from the Slip law fit to the 2-order step in p1060 is around 80, but we trust this estimate more because the data look very much like an "ideal" velocity step and the Slip law fit is excellent. The largest velocity increase in data set p1180 (Figures 6a and 6b) pushed the Slip law $V\theta/D_c$ to $\sim$ 300, equivalent to a velocity step of $\sim$ 2.5 orders of magnitude. The parameter inversions were constrained to a fixed stiffness ($k = 0.0012\,\mu\text{m}^{-1}$ for both p1169 and p1180) based on the short-term stress response to the reslide following a load point velocity hold performed later during both experimental runs. All the fits were also constrained at a fixed $a - b$ value (≈ 0.00025 for p1169 and ≈ 0.00001 for p1180) based on the steady state response from the data.

We again used the downhill simplex algorithm for the preliminary fits. The Aging law again does the worst job of all the laws considered here (Figures 5a and 6a). The Slip law produces a much better fit than the Aging law but a less impressive fit than for the 1–2 orders of magnitude steps in p1060. Interestingly, even though these experiments were carried out on the same starting material, the value of $D_c|_{\text{Slip}}$ obtained for the simulated gouge in p1169 is more than twice the value inferred for either p1060 or p1180. Recent laboratory experiments suggest that such variations in D_c might be due to differences in the extent of shear localization

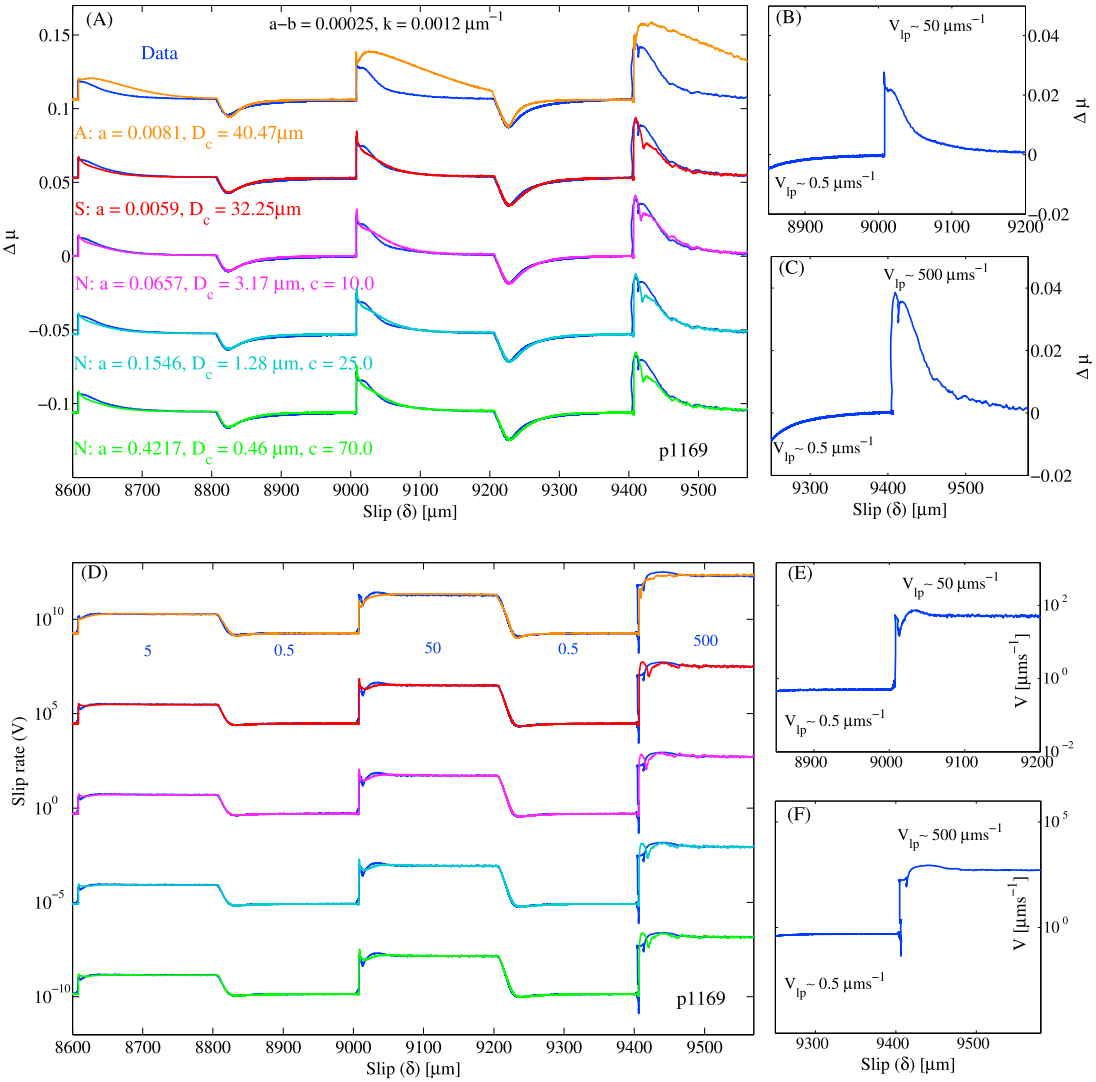

Figure 5. Fits to a sequence of large velocity steps (data set p1169) on simulated gouge. From left to right in Figures 5a and 5d: 1-order and 2-order step increases/decreases and an approximately 3-order velocity step increase. (a) The fit to $\Delta\mu$ values. (b, c) Observed $\Delta\mu$ values across the attempted 2-order and 3-order velocity increases, respectively. The complicated responses near peak stress can be seen. (d) The corresponding slip rates (V) predicted by the forward model for the fits to the $\Delta\mu$ time series in Figure 5a. (e, f) Slip rates calculated from the data for the attempted 2-order and 3-order velocity increases, respectively. Blue represents data in all panels. In Figures 5a and 5d, ochre: Aging law; red: Slip law; purple: Nagata law with $c = 10$; cyan: Nagata law with $c = 25$; green: Nagata law with $c = 70$. The numbers in blue in Figure 5d denote load point velocities in μms^{-1}.

and fabric development within the gouge sample [*Rathbun and Marone*, 2013]. Also, our choice of stressing rate-dependent weights (refer to the supporting information) led to the Aging law fitting the velocity step decreases better in p1169 and the step increases better for p1180. But the asymmetry in the Aging law response clearly prohibits it from fitting both the step increases and decreases as well as the Slip law. The Aging and Slip law solutions correspond to global minima for both p1169 and p1180. This was verified by choosing various initial parameter sets for the downhill simplex algorithm and, also, independently running the aforementioned Markov chain Monte Carlo (MCMC) code.

The MCMC posterior search revealed that the Nagata law fits accepted at the specified level of data error spanned many orders of magnitudes of values of c for both p1169 and p1180 (Figures 7a–7i). For p1169 (maximum Slip law $V\theta/D_c \sim 750$), the posterior for c showed a strongly peaked region between $c \sim 5$ and 60 and a quasi-uniform tail for $c \gtrsim 70$ extending over many orders of magnitude (Figure 7c). When compared to the quasi-uniform region, the Nagata law fits represented by the peaked region represented smaller RMSE values with $c \approx 10$ leading to the global minimum RMSE. This is similar to the posterior structure observed for

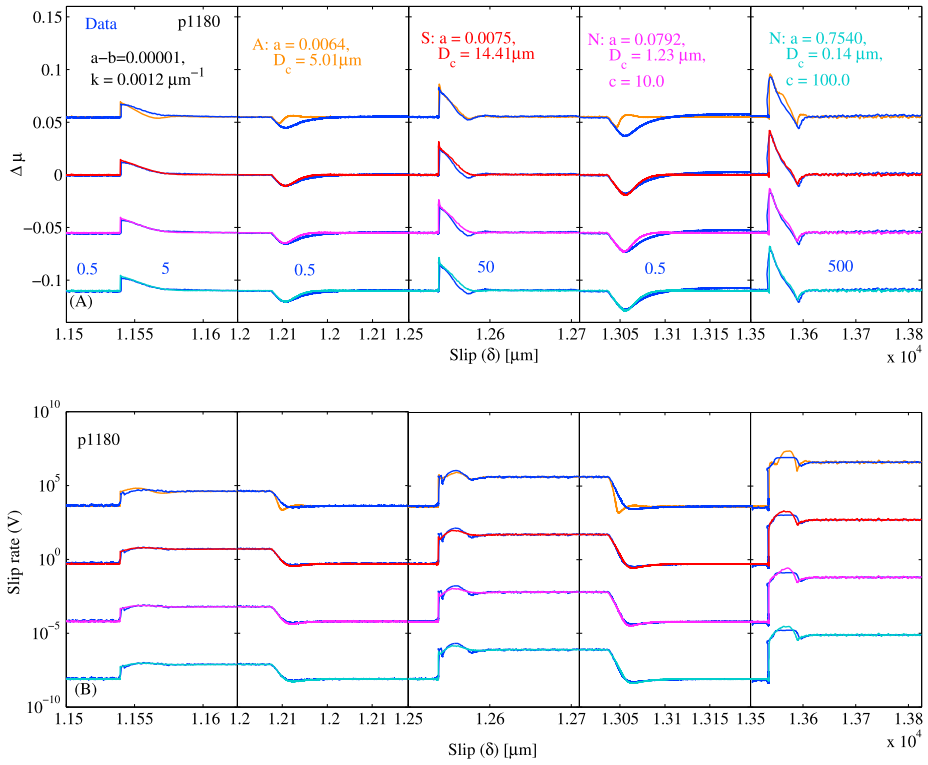

Figure 6. Fits to a sequence of large velocity steps on simulated gouge (data set p1180). From left to right in Figures 6a and 6b: 1-order and 2-order step increases and decreases with an attempted 3-order velocity step up at the end that pushed $V\theta/D_c \sim 300$ for the best fitting Slip law. (a) The fit to $\Delta\mu$ values. (b) The corresponding slip rates (V) predicted by the forward model for the best fitting $\Delta\mu$ time series. Blue: data; ochre: Aging law; red: Slip law; purple: Nagata fit with $c = 10$; cyan: Nagata fit with $c = 100$. The numbers in blue in Figure 6b denote load point velocities in μms^{-1}. For the Aging law, the data are plotted over the numerical results to facilitate its viewing.

p1060 in Figure 3c. The Nagata law fit for $c = 10$ is visually not identical to the Slip law fit, as can be clearly seen in Figure 5a. When compared to the Slip law fit, the Nagata law fit for $c = 10$ seems to have done a worse job of fitting the 2 orders of magnitude velocity increase but a better job for the ~3 orders of magnitude increase. The lower bound on c to produce fits identical to the Slip law, which we recognize as the onset of the quasi-uniform tail region in the posterior distribution, is around 70. This value is smaller than $c \sim 100$, the corresponding lower bound for p1060. Additionally, the best Nagata law fit needs $c \sim 10$ whereas this value was ~20 for p1060 (Figures 7c and 7f). Finally, the global lower bound on c for fits similar to the Slip law is also smaller for p1169 (~5) than it is for p1060 (~10). This appears to contradict our analytical expectations given the apparently larger departure from steady state in p1169 than p1060. However, it is worth pointing out that the stress data in p1169 show rather complicated behavior near peak stress for both the attempted 2-order and 3-order velocity increases (Figures 5b and 5c). Our analytical expectations might be too simplistic to explain the features of the numerical fits to such data sets that deviate this strongly from ideal velocity steps.

For p1180 (maximum Slip law $V\theta/D_c \sim 300$), the posteriors for a, D_c, and c were purely quasi-uniform beyond $c \sim 100$ and showed no prominent peaked regions around $c \sim 10$ like the ones seen for p1060 and p1169. In particular, the Nagata law with $c \approx 10$ led to worse fits than the Slip law, the most pronounced differences occurring between the fits to the 1-order and 2-order load point velocity step decreases (Figures 8a and 8b). There seems to be no region of the parameter space that allows the Nagata law to produce fits that have a lower RMSE than the best Slip law fit, at least when $a - b$ is constrained by the observed steady state behavior. The lower bound on c for generating fits identical to the Slip law appears to be ~100. This lower bound is the same as that found for p1060 (with a smaller apparent maximum excursion from steady state) and larger than ~70 as seen for p1169 (with a larger apparent maximum excursion from steady state).

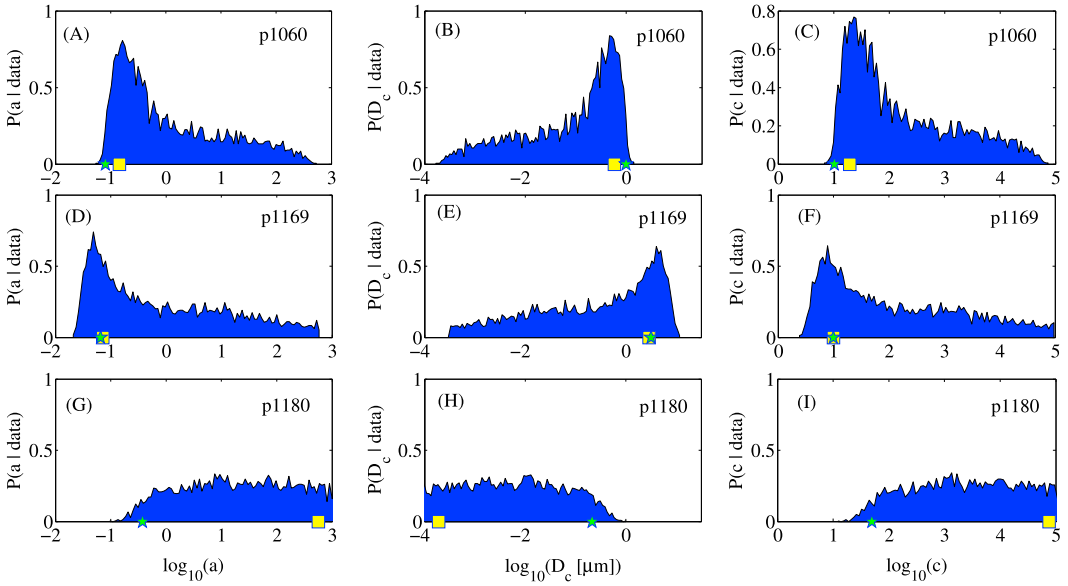

Figure 7. Nagata law posteriors for a, D_c, and c for data sets (a–c) p1060, (d–f) p1169, and (g–i) p1180. The green stars show the initiation point for the chain, and the yellow squares show the parameter values corresponding to the global minimum RMSE fit. The value of c was constrained to be less than some different upper bound a priori for each chain. This leads to the truncation of the quasi-uniform tails of the posteriors of c (the effects of this truncation is also seen in the posteriors of a and D_c). Comparing the posteriors of c across the three data sets shows that the presence of a strongly peaked region is not a universal feature whereas the presence of a quasi-uniform region representing fits identical to the best fitting Slip law (see Appendix B) is universal.

4.2.3. Comparing Analytical and Inversion Results

The analyses in sections 4.2.1 and 4.2.2 show that (1) the Slip law fits the $\gtrsim$ 2-order velocity step data much better than the Aging law; (2) given the best Slip law fit to a particular data set, we can always find lower bounds on c such that the Nagata law fits these data either slightly better or identically well. It is important to recognize that we have no analytical expectations for those Nagata law fits which match the stress data better than the Slip law. We only note from our inversion results that when this class of Nagata law fits do exist (for data sets p1060 and p1169), they appear as a strongly peaked region of the posterior distribution representing a well-constrained minimum RMSE solution (see Appendix B). For both p1060 and p1169, this maximum aposteriori (MAP) value of c is considerably smaller than the minimum value required to replicate the best Slip law fit with the Nagata law. However, given that the frictional properties of simulated gouge have been known to vary systematically with the extent of shear displacement [*Marone*, 1998b; *Rathbun and Marone*, 2013; *Marone and Saffer*, 2015], we cannot rule out the possibility that the slightly worse (than the MAP Nagata law fit) Slip law fits might only be an artifact of drift of the material properties across the experimental run.

On the other hand, we do have some analytical expectations relevant to the Nagata law fits which exactly reproduce the best Slip law fits to a given velocity step data set. These expectations, however, come with the caveat that they were derived from analytical results on true velocity steps (section 3), a condition only approximately satisfied in our experiments. With this caveat, the main analytical predictions regarding these Slip-law-like fits are the following: (1) The values of c which allow such fits can only be constrained to a lower bound, and (2) this lower bound on c is an increasing function of the maximum velocity step size that we choose to fit. In Appendix B, we show that the quasi-uniform tail of the marginal posteriors for c in Figures 3 and 7 represent this family of Slip-law-like fits and that these quasi-uniform posteriors are only bounded by a minimum value of c. This is in agreement with expectation (1) above. But, contrary to expectation (2), the lower bounds on c imposed by the onset of the quasi-uniform regions in the posteriors do not show any robust positive correlation with the size of the largest velocity step being fit. In particular, the data set with the largest excursion from the steady state led to the smallest value for this lower bound ($c \sim 70$ for p1169). As pointed out above, it is possible that this particular analytical expectation, derived for true velocity steps, is not relevant to "approximate" laboratory velocity steps in general. On the other hand, inherent differences

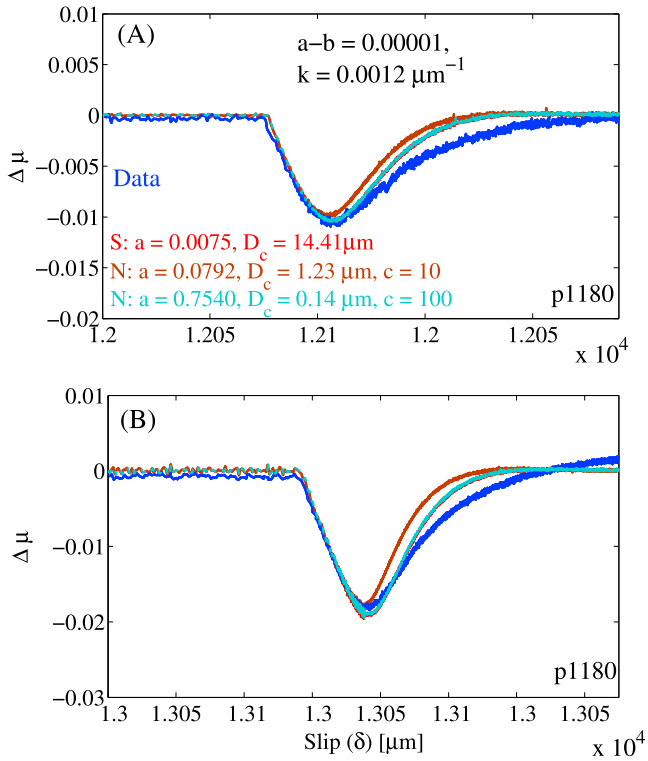

Figure 8. The fits to the (a) 1-order and (b) 2-order step decreases in load point velocity from data set p1180. Blue: data; red: Slip law; brown: Nagata fit with $c = 10$; cyan: Nagata fit with $c = 100$. The Slip law fit is identical to the Nagata fit with $c = 100$, and, hence, these fits lie on top of each other. This plot makes clear that the Slip law fits the data better than the Nagata law with $c = 10$. One needs $c \gtrsim 100$ in order to produce Nagata law fits identical to those produced by Slip law.

between the various experimental runs make comparison of trends difficult across the different data sets and could possibly mask any correlations. Therefore, to be sure whether expectation (2) was consistent with our inversions or not, we compared the lower bounds on c (for Slip-law-like fits) across different subsets of velocity steps from the same experimental run. We show in Appendix C that the lower bound on c (for Slip-law-like fits) derived from fitting only 1-order steps in each data set is always smaller than the corresponding estimate for the whole data set. This shows that the lower bound on c to produce Slip-law-like fits increases with the size of the velocity step being fit. That is, our inversion results on approximate velocity steps in the laboratory agree with our major analytical expectations based on ideal velocity steps.

5. Can There Be Too Large a Value of c?

Nagata et al. [2012] made micromechanical observations of the frictional surface but proposed a shear stress dependence of state which has no well-established micromechanical origin. In sections 3 and 4, we examined the implications of this additional factor in state evolution across a wide range of excursions from steady state sliding. The most striking of these implications is that velocity step data which is fit well by the Slip law is at least equally as well fit by the Nagata law over orders of magnitude variations in c larger than a minimum. Therefore, it is important to ask if there exists a physical constraint on the maximum, physically reasonable, value for c. One approach could be to find a proxy for c in the quantities which scale with c but have a clearer physical meaning and, hence, might be easier to constrain, e.g., the direct effect a. Because a scales linearly with c (equation (9b)), the value of a needed to fit the data increases to very large values as the value of c increases to $c \gg 1$ (e.g., for $c = 100$, the appropriate value of the Nagata law a for p1180 is $\sim$0.8). Unlike c, a has an independent physical interpretation based on only the friction law in equation (1): It determines the stress increase required to slip faster given a hypothetical fixed state (physical or chemical) of the slip surface. Assuming this direct velocity effect to be an activated Arrhenius rate process, the traditional room temperature Aging or Slip law estimate $a \sim 0.01$ corresponds to activation volumes of the order of

the molecular volumes of tectosilicates ($\sim 0.1\text{nm}^3$), provided contact stresses are assumed to be $\sim 1/10$ the shear modulus [*Rice et al.*, 2001; *Boettcher et al.*, 2007]. The *Nagata et al.* [2012] value of $a \sim 0.05$ on bare rock seems close enough to the order of magnitude theoretical value to be plausible. In fact, *Nagata et al.* [2012] have argued that $a \sim 0.05$ implies activation volumes which correspond to the typical Si-Si or Si-O bond lengths in tectosilicates (5 times smaller than the volumes corresponding to $a \sim 0.01$). However, it is not immediately clear if activation volumes of atomic order are physically preferable to those of molecular order, especially since the "preferred" value depends on the preferred physical mechanism behind the instantaneous rate effect. But atomic volumes seem to be a reasonable physical lower bound, and values of a larger than ~ 0.05 might already be pushing this boundary. Therefore, the value of $a \gtrsim 0.8$ appropriate to fit p1180 with $c \gtrsim 100$ is probably unreasonably large and raises the possibility that such large values of c could be falsified on this basis.

It should also be possible to test whether values of c as large as 10 (the minimum value required to fit the data in Figure 2 as closely as the Slip law) are plausible using acoustic monitoring of large velocity steps. For example, in Figure 2a the excursions in friction following the 2 orders of magnitude velocity steps are ~ 0.03. Given that the steady state friction coefficient in these experiments is ~ 0.6, this represents a roughly 5% change in frictional strength. From Figure 2b it appears that these velocity steps are sufficiently close to ideal that one can reasonably approximate the approach to steady state following the maximum stress excursion as occurring at constant slip speed. This implies that the stress change following the maximum excursion is due entirely to state evolution. If for concreteness we interpret state as true contact area, this implies a 5% change in contact area between the maximum stress excursion and the subsequent steady state.

Because this interpretation depends only upon the friction equation (1), it is independent of any state evolution law. However, we have already seen that the Nagata law implies an instantaneous change in state (contact area) across a stress step, and we can compare the magnitude of this change to the subsequent change with slip. The total stress change with slip can be determined by substituting $\delta = 0$ into either approximation (6) or (7), yielding (in agreement with the exact equation (14) in *Bhattacharya and Rubin* [2014])

$$\Delta\tau_{\text{slip}} = b\sigma\left(1 - \frac{c}{c+1}\frac{a}{b}\right)\ln\left(\frac{V_f}{V_i}\right). \tag{13}$$

The stress change associated with the instantaneous change in state can be determined from equation (9) in [*Bhattacharya and Rubin*, 2014]:

$$\Delta\tau_{\Delta\theta_{\text{inst}}} = a\sigma\frac{c}{c+1}\ln\left(\frac{V_f}{V_i}\right). \tag{14}$$

The ratio of the instantaneous area change to the subsequent area change with slip is then equal to $\Delta\tau_{\Delta\theta_{\text{inst}}}/\Delta\tau_{\text{slip}}$, or

$$\frac{\Delta A_{\text{inst}}}{\Delta A_{\text{slip}}} = \frac{\frac{c}{c+1}\frac{a}{b}}{1 - \frac{c}{c+1}\frac{a}{b}}. \tag{15}$$

This shows that for $a \sim b$ the instantaneous area change is larger than the subsequent evolution for all $c \gtrsim 1$. For the $c = 10$ required to fit the friction data with the Nagata law, the instantaneous area change should be 10 times the subsequent evolution. Given that ultrasonic transmissivity was shown to detect apparent changes in contact area associated with different steady state sliding velocities in the bare rock experiments of *Nagata et al.* [2012, 2014], such a large change should be easily visible.

6. Summary and Conclusions

Numerical simulations show that the feature of a state evolution law most relevant to nucleation of earthquakes is its response to large velocity increases [*Ampuero and Rubin*, 2008; *Bhattacharya and Rubin*, 2014]. To find the state evolution law most suitable for earthquake nucleation simulations, our study examines the extent to which the Aging, Slip, and Nagata laws can fit laboratory data comprising velocity steps of up to nearly 3 orders of magnitude on simulated gouge. Interpretation of earlier experimental work on generally smaller velocity steps suggest that the Slip law does a much better job of matching velocity step data than the linear slip weakening predicted by the Aging law far above steady state [*Ruina*, 1980; *Tullis and Weeks*, 1986]. On the other hand, for a given value of c the Nagata law predicts a transition from Slip to Aging law

behavior with increasing velocity step size [*Bhattacharya and Rubin*, 2014]. Since our experiments on simulated gouge pushed the sliding surface farther above steady state than prior laboratory experiments, this data set provided us a unique opportunity to examine the extent to which each of these laws explain rock friction data far above steady state. Additionally, given that our experiments pushed the sliding surface further from steady state than those of *Nagata et al.* [2012], we wanted to see if this led to the appropriate value of c for our experiments being different from the *Nagata et al.* [2012] value of 2.

Our data sets contained velocity steps of 1, 2, and nearly 3 orders of magnitude, all designed to produce close to ideal velocity steps in order to facilitate comparisons with theoretical predictions. We observed that the Slip law fits all of these data sets well and much more closely than the Aging law. The Nagata law parameters could always be suitably tuned to produce fits either slightly better than or equivalent to the best Slip law fits. But such Nagata law fits could only be generated for c in the range 10–100 which is significantly larger than the $c \sim 2$ value reported by *Nagata et al.* [2012] for initially bare rock surfaces. For all our data sets, the inversion algorithm could only constrain the minimum bound on c such that the Nagata law fit was at least as good as the Slip law. This and the fact that these lower bounds were also observed to be increasing functions of the size of the largest velocity step being fit, consistent with surfaces well described by the Slip law, raise questions about whether c is a physically based material parameter.

We conclude that both the Slip law and Nagata constitutive laws adequately describe velocity step tests. However, given a parsimonious view of free parameters, we prefer the Slip law. In detail, the Nagata law can fit velocity step data as well as or slightly better than the Slip law with the value of c larger than a minimum bound according to the size of the largest step size being fit. In fact, if one were to accept the Nagata law fit to p1180 for $c = 10$ as "close enough" to that for $c = 100$, our data cannot rule out the possibility that the Nagata law with $c \sim 10$ and $a \sim 0.07–0.08$ is appropriate for gouge. But we find it significant that given the additional parameter c introduced by the Nagata law, for the two experiments fit most closely by the models (p1060 and p1180), the inversion chooses to make that additional parameter large enough that the Nagata law appears nearly indistinguishable from the Slip law.

It is important to note that our data sets were designed specifically to study the response of the sliding surface to large velocity steps. This style of experiments has long been known to favor the Slip law, albeit with generally smaller velocity steps. More investigation of experimental data that also contain sequences of slide-hold-reslides is required to find which of the prevalent state evolution laws best explains all the robust features of laboratory friction. More experiments should also be carried out to fully understand the stress dependence of state and the large values of a, found by *Nagata et al.* [2012] for bare rocks.

Appendix A: Estimating Stiffness From Data

In friction experiments, the effective stiffness of the experimental configuration depends upon the testing machine, the loading assembly, and the sample. Thus, the effective stiffness can vary depending on the material being used [*Leeman et al.*, 2015]. This makes it necessary to estimate the stiffness (k in equation (11)) individually for each data set, because stiffness may vary systematically with shear strain, sample damage, or other factors [*Berthoud and Baumberger*, 1998; *Leeman et al.*, 2015]. However, for our current work we neglect any such effect and treat k as constant during our experiments. In order to estimate this constant stiffness, we note that immediately following a large load point velocity increase one can write

$$\Delta\mu = k(\delta_{lp} - \delta) = k\delta_{lp}\left(1 - \frac{\delta}{\delta_{lp}}\right) \approx k\delta_{lp}, \tag{A1}$$

where δ and δ_{lp} are surface and load point displacements since the velocity increase, respectively, and instantaneously $\delta/\delta_{lp} \ll 1$ for a sufficiently large velocity increase. A linear fit to the $\Delta\mu$ versus δ_{lp} plot over the first few data points gives k as the slope (Figure A1). Another approach is to simultaneously invert for k during the inversion. The problem with this approach is that one needs to apply large weights on the misfits to the short-term stress response to velocity increases in order to best constrain the stiffness estimate. However, for some data sets (like p1060), simultaneous inversion (with a state evolution law that fits the data well, e.g., the Slip law for p1060) constrains k to within a few percent of the linearized estimate even without such special weighting schemes.

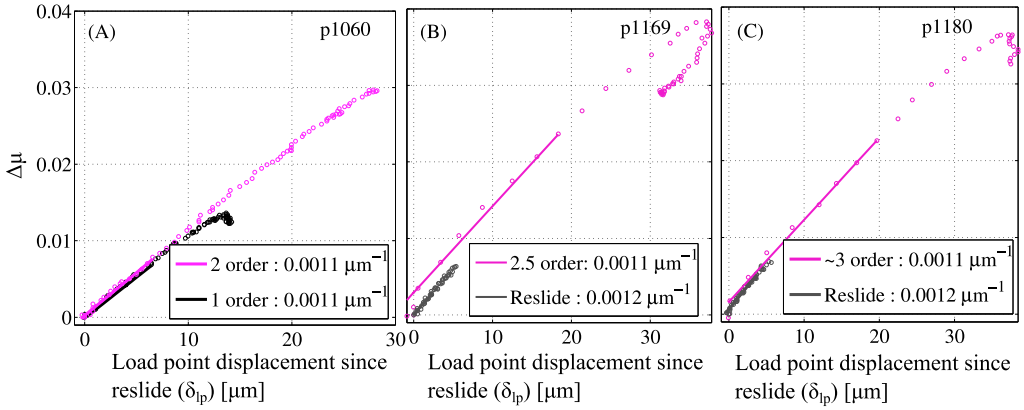

Figure A1. Stiffness estimation for the different data sets. The initial portion of the excursion of $\Delta\mu$ following a large velocity increase or reslide following a hold (if performed during the same experimental run) is used to estimate the stiffness. The slope of a linear fit to the $\Delta\mu$ versus δ_{lp} plot yields the stiffness if $V_f/V_i \gg 1$, with V here referring to the load point velocity.

Appendix B: The Structure of the Nagata Law Posterior for p1060

In section 4.2.1 and Figure 3, we have seen how the posterior distribution of c for p1060 shows a strongly peaked region and a quasi-uniform region. In this section we will try to understand the nature of the fits that represent the two regimes. We already have some a priori notion of the structure of the posterior by exploring the parameter space with the downhill simplex algorithm over orders of magnitude variations in c. To carry out this analysis, we typically fix $a - b$ and c and vary a and D_c with the downhill simplex to obtain the best Nagata law fit for a given value of c. Two main features were observed: (1) For $c \sim 10-50$ the Nagata law fits can be tuned to look slightly better than the best Slip law fit. (2) For $c \gtrsim 100$, the Nagata law parameters can be tuned to exactly reproduce the best Slip law fit. Therefore, it is reasonable to expect that the posterior of c is likely unbounded along c with each value of $c \gtrsim 10$ corresponding to a fit with varying levels of support from the data.

In order to quantify the visual qualities of the two regimes of the Nagata law fits from a Bayesian perspective, we first need to specify a value of S_e in the framework described in the supporting information. We choose the maximum of the standard deviations obtained by analyzing the fluctuations in shear stress about steady state frictional strength (Figure S1) therein. This value, $S_e = 0.00045$, is a lower bound on the data error. Running the Markov chain at this level data error leads to tightly bounded Gaussian posteriors for a, D_c, and c in Figure B1. All the parameter values from this chain lead to fits which "look" better than the best Slip law fit. The smallest value of the S_e at which the Nagata posteriors started showing the unbounded structures was around 0.004, i.e., about 10 times the value obtained from the error analysis of the steady state portions of the shear stress curves. It is noteworthy that the gross features of the posterior stayed persistent even when we used a value of S_e a few times this value. We used this value of S_e for the Markov chain showed in Figure 3. At this value, the Markov chain shows a strongly peaked region and a quasi-uniform tail for the posteriors. Given that the a, D_c, and c values representing the peak are coincident with the means of the Gaussians in Figures B1a–B1c, we identify this peaked region as representing the global minimum of the Nagata law RMSE. These belong to the family of Nagata law fits to p1060 which look slightly better than the Slip law.

The next task is to describe the family of Nagata law fits to p1060 which are exactly identical to the best Slip law fit. The easiest way to do this was to fit the best Slip law fit to p1060 with the Nagata law. In other words, we generated the shear stress profile for the best Slip law fit to p1060 and added Gaussian white noise with standard deviation 0.00045. This "synthetic" data set was then analyzed using Markov chains with $S_e = 0.00045$. This clearly reveals a quasi-uniform distribution for $c \gtrsim 100$ (Figures B1d–B1f). This shows that the quasi-uniform tail of the Markov chain in Figure 3 represents the Nagata law fits which are exactly identical to the best Slip law fit to p1060.

Before concluding this appendix it is important to recognize that it is our choice of S_e that allows the unbounded structure of the Nagata law posteriors in Figure 3 to be revealed. Choosing $S_e = 0.00045$ would have led to well-bounded Gaussian posteriors. One reason to choose larger values of S_e is that the friction

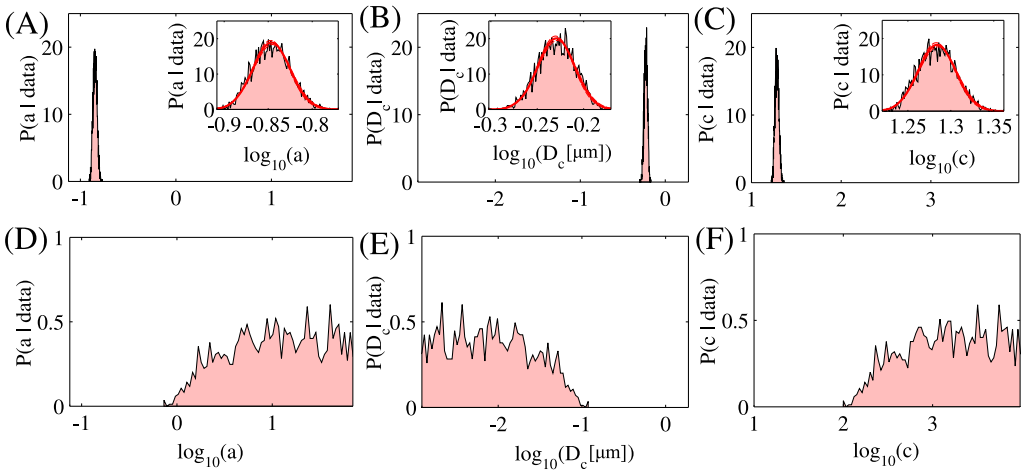

Figure B1. (a–c) The Nagata law posteriors for a, D_c, and c for data set p1060 with $S_e = 0.00045$ (the maximum standard deviation from the steady state error distributions constructed in Figure S1 in the supporting information). The posteriors are well-bounded Gaussians as shown in the inset by overlaying maximum likelihood estimates and the corresponding 5% error bounds as red solid and dashed lines, respectively. The mean of these Gaussians coincide exactly with the parameter values representing the global minimum of the Nagata law RMSE for the chain in Figure 3 which was run with $S_e = 0.004$. This helps us identify the strongly peaked regions in the posteriors in Figure 3 with these bounded Gaussians whose precise structure emerges at this stricter constraint on data error. (d–f) The Nagata law posteriors for a, D_c, and c for fits to the best Slip law fit to data set p1060 at the same standard error as Figures B1a–B1c. The posteriors reveal a quasi-uniform distribution with a well-defined lower bound on c. This lets us recognize the quasi-uniform tails in the posteriors in Figure 3 as Nagata law fits which are identical to the best Slip law fit.

values across small numbers of repeated experiments typically show much larger fluctuations than those characterized by our analysis of the steady state portions, with S_e easily up to an order of magnitude larger for common granular materials [see *Rathbun and Marone*, 2013, Figures 4 and 5]. Additionally, the choice of a scalar standard error is anyways a gross oversimplification as consecutive data points sampled under nonsteady sliding are strongly correlated. Most importantly, the magnitude of modeling errors are much larger than the random fluctuation of data under steady state sliding. In other words, we assume that these friction constitutive equations are fundamentally deficient in describing the detailed features of laboratory experiments, and, therefore, modeling error is the dominant source of misfit. In this sense, the estimate of S_e from the analysis of steady state sliding also leads to a lower bound on the estimate of modeling error as the model predicts constant steady state frictional strength. Then assuming data error to be negligible when compared to modeling error, one should naturally choose larger values of S_e for poorly fit data. But as a practical strategy, we ran a number of chains with S_e between 10 and 40 times the value estimated from steady state sliding (perhaps by chance, this is also the range typically represented by the variations in frictional strength across the repeated experiments of *Rathbun and Marone* [2013]). We then chose the minimum of these trial values of S_e such that the posteriors did not change their gross shapes even when higher values from this range were used as S_e. These values of S_e always led to posteriors which were consistent with the features of the model parameter space revealed by probing the distribution of local minima over many orders of magnitude variations in c using the downhill simplex algorithm. For the Markov chains corresponding to p1169 (Figures 7d–7f), the estimate of S_e from the steady state analysis was around 0.00025 while the value used was 0.008. Similarly for p1180, the steady state estimate of S_e was ~0.0003 while we used the value 0.003 to construct the Markov chains in Figures 7g–7i. It is interesting that this pragmatic approach also leads to the largest S_e being chosen for the worst fit data set, p1169.

Appendix C: Does the Minimum Bound on *c* for Producing Slip-Law-Like Fits Increase With the Size of Velocity Steps?

As described in sections 4.2.1–4.2.3, our inversions of the laboratory velocity step data show that the lower bound on the value of c, above which the Nagata law can replicate the best Slip law fit to each data set, shows no correlation with the size of the largest velocity step being fit. In contrast, our theoretical results predict that this lower bound should increase with the size of the velocity step being fit (see section 3). This disagreement between theory and inversion could be due to the fact that the experiments represent velocity

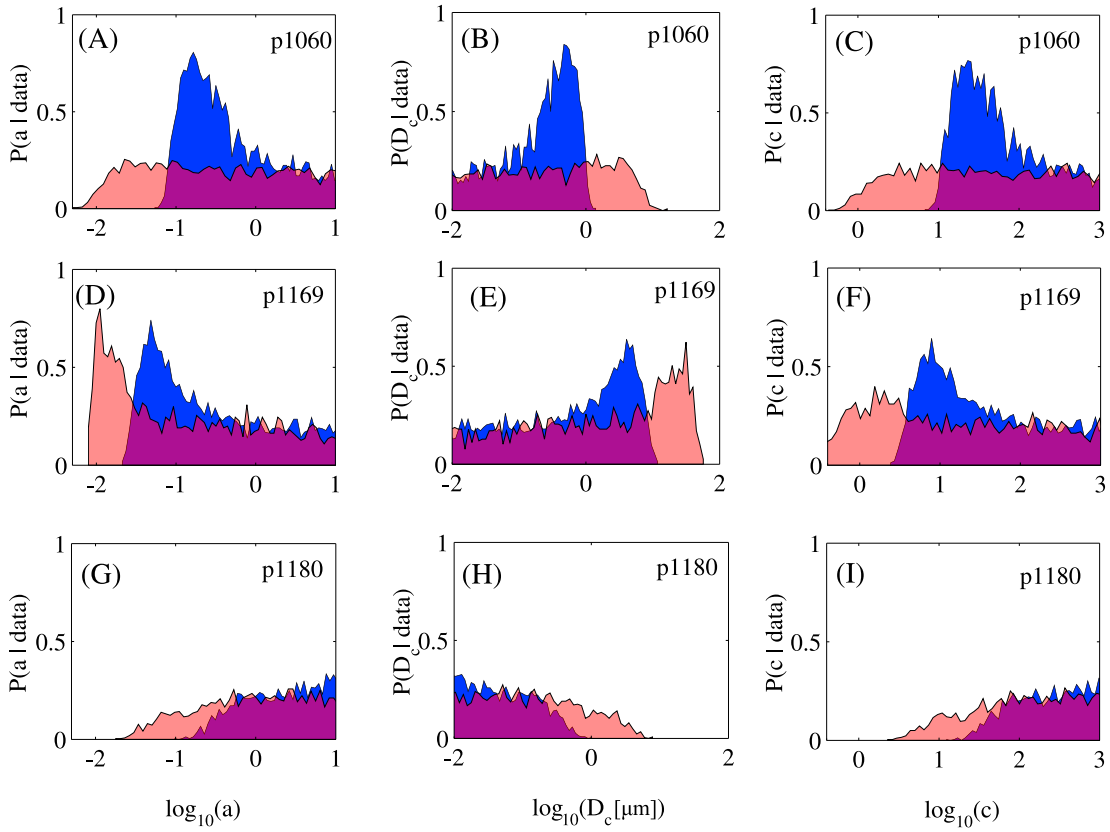

Figure C1. The Nagata law posteriors for a, D_c, and c for data sets (a–c) p1060, (d–f) p1169, and (g–i) p1180. The posterior distributions in blue in the background are the same as those in Figure 7; i.e., they represent the MCMC samples drawn for the whole data set. The semitransparent red posteriors in the foreground represent fits to only the 1 order of magnitude steps in the respective data sets at the same level of standard error as the blue posteriors. It is clear that the lower bound on c for producing Nagata law fits at least as good as the best Slip law fit to the 1 order of magnitude steps only is smaller than the corresponding bound for the fits which also include the two- or larger order steps. Additionally, the lower bound on c to produce Nagata law fits identical to the best Slip law fits is also smaller when fitting only 1 order of magnitude steps. This lower bound on c is marked approximately by the onset of the quasi-uniform region of the posterior distribution of c.

steps only approximately, and, hence, the analytical results might not be relevant. On the other hand, the expectation that a positive correlation between the minimum bound on c (for Slip-law-like fits) and the size of the velocity steps being fit would be apparent across the experimental runs implicitly assumes that these data sets differ only in the size of velocity steps they contain. But there do exist other differences, e.g., the Slip law parameters obtained from the three experimental runs do not agree with each other, particularly p1169 leading to estimates of D_c almost twice as large as the estimates from p1060 and p1180. Therefore, it might be possible that even though our analytical expectations are relevant to the approximate experimental velocity steps, the predicted correlations across these data sets might be suppressed by the inherent (also possibly experimental) differences between them. In the rest of this section we show that this is indeed the case.

If the analytical expectations from ideal velocity steps indeed apply to laboratory data, comparing the lower bounds on c (for Slip-law-like fits) across different subsets of velocity steps from the same experimental run should reveal larger lower bounds for larger velocity steps. To show this, we ran the Nagata law MCMC posterior search on only the 1-order steps from each of the three data sets. Comparing these posteriors to those derived from the corresponding whole data sets, we observed that for all three experimental runs, the lower bounds on c (to produce fits identical to the Slip law) were smaller for the 1 order of magnitude steps ($c \sim 1$ for p1060, $c \lesssim 7$ for p1169 and $c \sim 10$ for p1180) than for the whole data sets (Figures C1c, C1f, and C1i). Note that in Appendix B we have established that the quasi-uniform region of the posterior for c represents Nagata law fits identical to the best Slip law fits to the respective data sets, and the stated lower bounds represent the onset of quasi-uniformity. These results show that, for given velocity step data, the lower bound on c for producing Nagata law fits identical to the best fitting Slip law indeed increases with the size of the largest step being fit, a conclusion that agrees with our analytical prediction.

Note, for p1169, that the posterior for c obtained by fitting only 1-order steps shows a weakly peaked region while those for a and D_c show very clear, well-constrained, peaked regions (Figures C1d–C1f). The lower bound of the weakly peaked region in the posterior for c goes to values of $c \ll 1$. This regime of fits is equivalent to the best Aging law fit to the data. In fact, for all $c \ll 1$, the Nagata law reproduces the best Aging law fit to the data for a particular combination of a and D_c which show up as the peaks in the respective posteriors. Therefore, there is no strict lower bound on c when one exclusively fits the 1-order steps in p1169 (at our specified level of data error). In this case, we imposed an artificial lower bound in our inversions through the choice of the prior.

Acknowledgments
P.B. thanks David Medvigy for introducing him to many of the techniques of Bayesian inference used in this study. All the data used in this study are available upon request from the authors. This research was supported by the U.S. Geological Survey (USGS), Department of the Interior, under USGS awards G14AP00026 and G15AP00037. The views and conclusions contained in this document are those of the authors and should not be interpreted as necessarily representing the official policies, either expressed or implied, of the U.S. Government.

References

Ampuero, J. P., and A. M. Rubin (2008), Earthquake nucleation on rate and state faults — Aging and slip laws, *J. Geophys. Res.*, *113*, B01302, doi:10.1029/2007JB005082.
Bai, Y. (2009a), An adaptive directional Metropolis-within-Gibbs algorithm, *Tech. Rep.*, Univ. of Toronto, Toronto, Canada.
Bai, Y. (2009b), Convergence of adaptive Markov chain Monte Carlo algorithms, PhD thesis, Univ. of Toronto, Toronto, Canada.
Bayart, E., A. M. Rubin, and C. Marone (2006), Evolution of fault friction following large velocity jumps, *Eos Trans. AGU*, *87*(52), Fall Meet. Suppl., Abstract S31A–0180.
Beeler, N. (2007), *Laboratory-Observed Faulting in Intrinsically and Apparently Weak Materials*, chap. 13, pp. 370–449, Columbia Univ. Press, New York.
Beeler, N., T. E. Tullis, and J. D. Weeks (1994), The roles of time and displacement in the evolution effect in rock friction, *Geophys. Res. Lett.*, *21*, 1987–1990.
Berthoud, P., and T. Baumberger (1998), Shear stiffness of a solid–solid multicontact interface, *Proc. R. Soc. A*, *454*(1974), 1615–1634, doi:10.1098/rspa.1998.0223.
Berthoud, P., T. Baumberger, C. G'Sell, and J.-M. Hiver (1999), Physical analysis of the state- and rate-dependent friction law: Static friction, *Phys. Rev. B*, *59*, 14,313–14,327, doi:10.1103/PhysRevB.59.14313.
Bhattacharya, P., and A. M. Rubin (2014), Frictional response to velocity steps and 1-D fault nucleation under a state evolution law with stressing-rate dependence, *J. Geophys. Res. Solid Earth*, *119*(3), 2272–2304, doi:10.1002/2013JB010671.
Bhattacharya, P., A. M. Rubin, and N. Beeler (2014), Do laboratory slide-hold-slide experiments really provide evidence for time-dependent healing in rock?, paper presented at 25th SCEC Annual Meeting Proceedings, SCEC., Abstract 139.
Blanpied, M. L., C. J. Marone, D. A. Lockner, J. D. Byerlee, and D. P. King (1998), Quantitative measure of the variation in fault rheology due to fluid-rock interactions, *J. Geophys. Res.*, *103*(B5), 9691–9712.
Boettcher, M. S., G. Hirth, and B. Evans (2007), Olivine friction at the base of oceanic seismogenic zones, *J. Geophys. Res.*, *112*, B01205, doi:10.1029/2006JB004301.
Dieterich, J. H. (1972), Time-dependent friction in rocks, *J. Geophys. Res.*, *77*(20), 3690–3697.
Dieterich, J. H. (1978), Time-dependent friction and the mechanics of stick-slip, *Pure Appl. Geophys.*, *116*(4–5), 790–806.
Dieterich, J. H. (1979), Modeling of rock friction: 1. Experimental results and constitutive equations, *J. Geophys. Res.*, *84*, 2161–2168.
Dieterich, J. H. (1981), Constitutive properties of faults with simulated gouge, in *Mechanical Behavior of Crustal Rocks: The Handin Volume*, edited by N. L. Carter et al., chap. 8, pp. 103–120, AGU, Washington, D. C., doi:10.1029/GM024p0103
Dieterich, J. H., and B. D. Kilgore (1994), Direct observation of frictional contacts: New insights for state-dependent properties, *Pure Appl. Geophys.*, *143*, 283–302.
Guan, Y., R. Fleissner, P. Joyce, and S. M. Krone (2006), Markov chain Monte Carlo in small worlds, *Stat. Comput.*, *16*(2), 193–202, doi:10.1007/s11222-006-6966-6.
Karner, S. L., and C. Marone (2001), Fractional restrengthening in simulated fault gouge: Effect of shear load perturbations, *J. Geophys. Res.*, *106*(B9), 19,319–19,337, doi:10.1029/2001JB000263.
Leeman, J., M. M. Scuderi, C. Marone, and D. M. Saffer (2015), Stiffness evolution of granular layers and the origin of repetitive, slow, stick-slip frictional sliding, *Granular Matter*, *17*, 447–457.
Li, Q., T. E. Tullis, D. Goldsby, and R. W. Carpick (2011), Frictional ageing from interfacial bonding and the origins of rate and state friction, *Nature*, *480*(7376), 233–236.
Linker, M. F., and J. H. Dieterich (1992), Effects of variable normal stress on rock friction: Observations and constitutive equations, *J. Geophys. Res.*, *97*(B4), 4923–4940.
Marone, C. (1998a), The effect of loading rate on static friction and the rate of fault healing during the earthquake cycle, *Nature*, *391*, 69–72.
Marone, C. (1998b), Laboratory derived friction laws and their application to seismic faulting, *Annu. Rev. Earth Planet. Sci.*, *26*, 643–696.
Marone, C., and D. M. Saffer (2015), The mechanics of frictional healing and slip instability during the seismic cycle, in *Treatise on Geophysics*, vol. 4, 2nd ed., edited by G. Schubert, pp. 111–138, Elsevier, Oxford, U. K.
Nagata, K., M. Nakatani, and S. Yoshida (2012), A revised rate- and state-dependent friction law obtained by constraining constitutive and evolution laws separately with laboratory data, *J. Geophys. Res.*, *117*, B02314, doi:10.1029/2011JB008818.
Nagata, K., B. D. Kilgore, N. Beeler, and Nakatani M (2014), High-frequency imaging of elastic contrast and contact area with implications for naturally observed changes in fault properties, *J. Geophys. Res. Solid Earth*, *119*, 5855–5875, doi:10.1002/2014JB011014.
Nakatani, M. (2001), Conceptual and physical clarification of rate and state friction: Frictional sliding as a thermally activated rheology, *J. Geophys. Res*, *106*(B7), 13,347–13,380.
Nakatani, M., and H. Mochizuki (1996), Effects of shear stress applied to surfaces in stationary contact on rock friction, *Geophys. Res. Lett.*, *23*(8), 869–872, doi:10.1029/96GL00726.
Press, W. H., S. A. Teukolsky, W. T. Vetterling, and B. P. Flannery (1996), *Numerical Recipes in Fortran 90: The Art of Parallel Scientific Computing*, 2nd ed., Cambridge Univ. Press, New York.
Rathbun, A. P., and C. Marone (2013), Symmetry and the critical slip distance in rate and state friction laws, *J. Geophys. Res. Solid Earth*, *118*, 3728–3741, doi:10.1002/jgrb.50224.
Rice, J. R. (1993), Spatio-temporal complexity of slip on a fault, *J. Geophys. Res.*, *98*(B6), 9885–9907.
Rice, J. R., N. Lapusta, and K. Ranjith (2001), Rate and state dependent friction and the stability of sliding between elastically deformable solids, *J. Mech. Phys. Solids*, *49*(9), 1865–1898, doi:10.1016/S0022-5096(01)00042-4.
Rosenthal, J. S. (2011), Optimal proposal distribution and adaptive MCMC, in *Handbook of Markov Chain Monte Carlo*, edited by S. Brooks et al., pp. 93–112, Chapman and Hall, Boca Raton, Fla.

Ruina, A. (1980), Friction laws and instabilities: A quasistatic analysis of some dry frictional behavior, PhD thesis, Div. of Eng., Brown Univ., Providence, Rhode Island.
Ruina, A. (1983), Slip instability and state variable friction laws, *J. Geophys. Res.*, *88*, 10,359–10,370.
Savage, H. M., and C. Marone (2007), Effects of shear velocity oscillations on stick-slip behavior in laboratory experiments, *J. Geophys. Res.*, *112*, B02301, doi:10.1029/2005JB004238.
Tullis, T. E., and J. D. Weeks (1986), Constitutive behavior and stability of frictional sliding of granite, *Pure Appl. Geophys.*, *124*(3), 383–414.